inorganics

MDPI

Article

Organoplatinum Chemistry Related to Alkane Oxidation: The Effect of a Nitro Substituent in Ligands Having an Appended Phenol Group

Anwar Abo-Amer [1,2], Mohamed E. Moustafa [1], Paul D. Boyle [1] and Richard J. Puddephatt [1,*]

[1] Department of Chemistry, University of Western Ontario, London, ON N6A 5B7, Canada
[2] Department of Chemistry, Al al-Bayt University, Mafraq 25113, Jordan
* Correspondence: pudd@uwo.ca

Abstract: The organoplatinum chemistry of the ligands 2-C_5H_4N-CH_2-NH-C_6H_3-2-OH-5-X (**L1**, X = H; **L3**, X = NO_2) and 2-C_5H_4N-CH=N-C_6H_3-2-OH-5-X (**L2**, X = H; **L4**, X = NO_2), which contain an appended phenol substituent, is described. Comparisons are made between the ligands with amine or imine groups (**L1**, **L3** vs. **L2**, **L4**) and ligands with X = H or NO_2 (**L1**, **L2** vs. **L3**, **L4**), and major differences are observed. Thus, on reaction with the cycloneophylplatinum(II) complex [{Pt($CH_2CMe_2C_6H_4$)(μ-SMe_2)}$_2$], ligands **L1**, **L2** and **L4** give the corresponding platinum(II) complexes [Pt($CH_2CMe_2C_6H_4$)(κ^2-*N*,*N*′-**L**)], containing a Pt··HO hydrogen bond, whereas **L3** gives a mixture of isomeric platinum(IV) hydride complexes [PtH($CH_2CMe_2C_6H_4$)(κ^3-*N*,*N*′,*O*-**L3-H**)], which are formed by oxidative addition of the phenol O-H bond and which react further with oxygen to give [Pt(OH)($CH_2CMe_2C_6H_4$)(κ^3-*N*,*N*′,*O*-**L3-H**)]. The differences in reactivity are proposed to be due to the greater acidity of the nitro-substituted phenol groups in **L3** and **L4** and to the greater ability of the deprotonated amine ligand **L3** over **L4** to stabilize platinum(IV) by adopting the *fac*-κ^3-*N*,*N*′,*O*-**L3-H** coordination mode.

Keywords: platinum; diimine; nitrophenol; hydrogen bond; oxygen activation

check for updates

Citation: Abo-Amer, A.; Moustafa, M.E.; Boyle, P.D.; Puddephatt, R.J. Organoplatinum Chemistry Related to Alkane Oxidation: The Effect of a Nitro Substituent in Ligands Having an Appended Phenol Group. *Inorganics* **2024**, *12*, 32. https://doi.org/10.3390/inorganics12010032

Academic Editors: Francis Verpoort, Claudio Pettinari, Maurizio Peruzzini, Richard Layfield, Rainer Winter, Moris S. Eisen, Gábor Papp, Shuang Xiao and Axel Klein

Received: 2 November 2023
Revised: 11 December 2023
Accepted: 10 January 2024
Published: 16 January 2024

1. Introduction

The catalysis of selective oxidation of organic compounds with oxygen typically requires, as key steps, C-H bond activation, dioxygen activation, combination of the M-C and M-O bonded fragments and elimination of the product to regenerate the active catalyst. There are still major challenges in discovering effective catalysts. Recent research is based on knowledge of the successful biological enzymes [1–6]. Thus, in catalysis, it is necessary that the oxidation by dioxygen to form a metal–oxygen bond is followed by a reduction step, involving its cleavage, and that both steps should occur rapidly [7–14]. For example, many noble metal complexes, such as those of palladium(II) [15–20] and platinum(II) [21–31], need to be activated in order to react with oxygen. For activation of electron-rich organoplatinum(II) complexes [PtR_2L_2], with R = alkyl or aryl and L = nitrogen-donor ligand, towards dioxygen, it is advantageous to use ligands with a third donor atom and/or a substituent containing a hydrogen bond donor group (usually an NH or OH group) [13,21–24,29,30,32–40]. In enzyme catalysis, a tyrosine substituent or water molecule can aid the oxygen-binding step by hydrogen bonding to an incipient superoxide or peroxide group [1–6], and a similar effect may explain the enhanced reactivity of organoplatinum complexes that have ligands with appended phenol substituents [33–40]. Such an activation of dioxygen can therefore be considered biomimetic.

The ligands used in the present work are shown in Scheme 1. The neutral ligands **L1**–**L3** have been shown to act as NN chelate ligands in platinum complexes [33–42] (Scheme 2). In electron-rich dimethylplatinum(II) or cycloneophylplatinum(II) complexes, the appended phenol substituents may form OH··Pt hydrogen bonds (***A***, ***B***, ***G***) or, with

the more acidic nitrophenol substituent in **L3**, oxidatively add to form a hydridoplatinum(IV) complex (***C*** and isomers) [37]. In all cases, the pendent phenol group promotes a reaction with dioxygen to give platinum(IV) complexes (***D***, ***E***, ***F***). The present work describes additional reactions of organoplatinum complexes with ligands **L1**–**L3** and extends the chemistry with cycloneophylplatinum complexes [35–54] and the nitro-imine ligand **L4** [55–58].

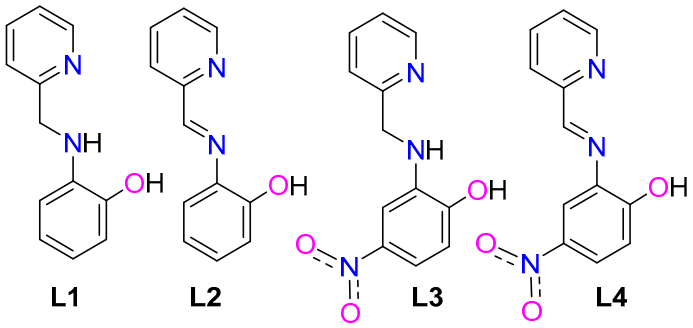

Scheme 1. The ligands used in this work.

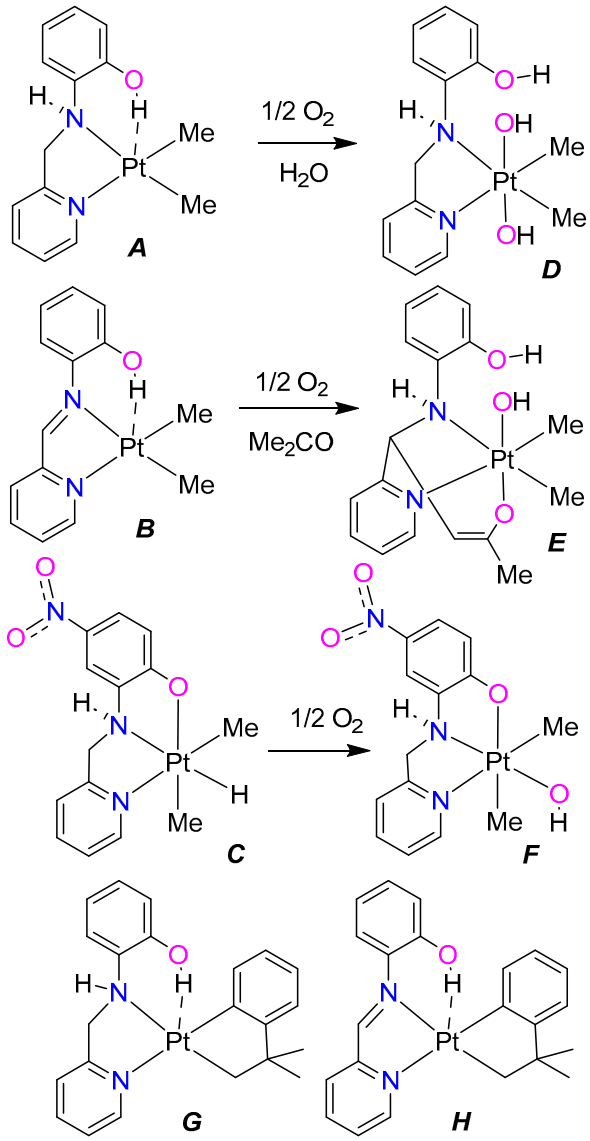

Scheme 2. Some platinum complexes of ligands **L1**–**L3**.

2. Results

2.1. The Ligand **L4**

The ligand **L4** is known to form coordination complexes, but it has usually been prepared and used in situ [55–57] and, since several related imine derivatives are known to cyclize to the corresponding oxazoline [58–61], it was prepared and studied in solution. In most solvents (CD_2Cl_2, $CDCl_3$, $(CD_3)_2CO$, $(CD_3)_2SO$ and CD_3CN), **L4** was present in the imine form as shown by the prominent singlet resonance for the imine N=CH proton (δ = 8.96 in CD_2Cl_2) in the ^{1}H NMR spectrum. However, in CD_3OD solution, an equilibrium mixture of **L4** and the oxazoline isomer **L5** was present in a ratio **L4**:**L5** = 1:4 (Figure 1). The imine resonance for **L4** was at δ = 8.93 and the corresponding proton for the oxazoline derivative **L5** was at δ = 5.86. Following the evaporation of the solution and the dissolution of the solid in CD_2Cl_2, the ^{1}H NMR spectrum showed that complete isomerization of **L5** back to **L4** had occurred. DFT calculations predict that the preferred structure of **L4** is the *E*–isomer [33], with the two nitrogen donor atoms (pyridyl and imine) in the *anti* conformation, whereas the *syn* conformation is required for chelation (calculated *E-anti* − *E-syn* = 3 kJ mol^{-1}). In the gas phase, **L4** is predicted to be more stable than **L5** by 23 kJ mol^{-1}, but the difference in energy is less in polar solvents and **L5** is calculated to be slightly more stable than **L4** in methanol, consistent with the experimental observations. The calculations take no account of specific intermolecular hydrogen bonding interactions so are not expected to be accurate, but the trend is clear.

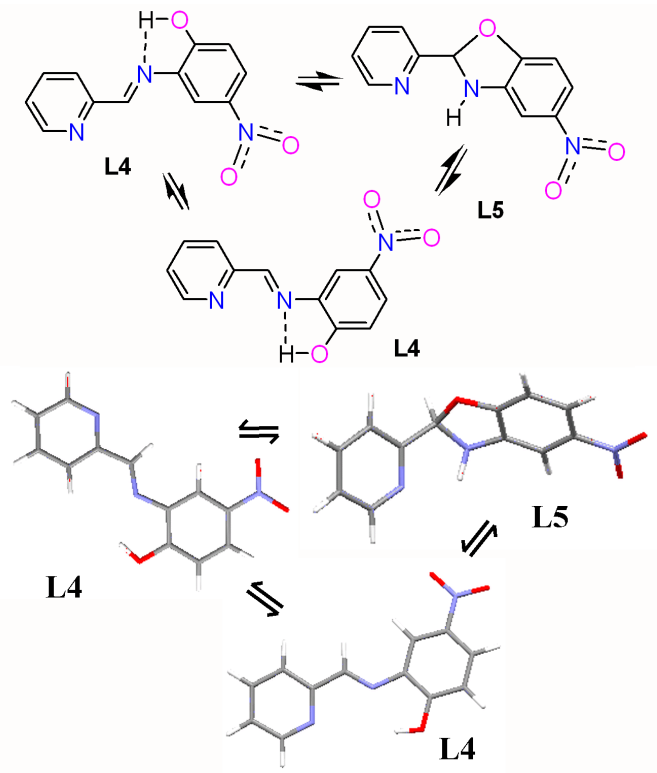

Figure 1. Conformers of **L4** and isomerization to oxazolyl derivative **L5**: (**above**), line drawings; (**below**), DFT-calculated structures.

2.2. Model Platinum(IV) Complexes with Imine Ligand **L2**

The reaction of the complex [$PtMe_2$(**L2**)], ***B*** (Scheme 2) [33] with methyl iodide or 3,5-di-*t*-butylbenzyl bromide gave the platinum(IV) complexes [$PtIMe_3$(**L2**)], **1**, or [$PtBrMe_2(CH_2C_6H_3$-3,5-*t*-Bu_2)(**L2**)], **2**, respectively (Scheme 3). The structures of complexes **1** and **2** (Figures 2 and 3) show that the **L2** remains as a bidentate ligand and that the phenol forms an intramolecular hydrogen bond OH··IPt in **1** and OH··BrPt in **2**. The geometrical constraints of the imine group make it difficult for the deprotonated **L2** to act

as a *fac*-*N*,*N*,*O*-tridentate ligand, as is often observed with the corresponding amine ligand **L1** [40,41]. This feature, which is established by the reactions of Scheme 2, will be important in later studies of reactivity with dioxygen. The platinum(IV) complexes **1** and **2** are chiral and this leads to non-equivalence of the benzylic CH_2 protons of complex **2**, which appear as an AB multiplet in the ^{1}H NMR spectrum.

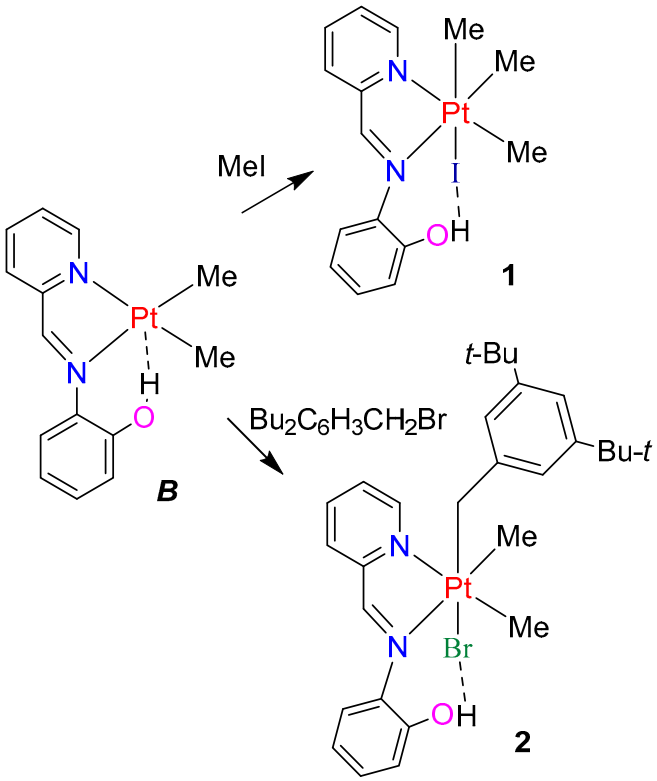

Scheme 3. Formation of the organoplatinum(IV) complexes **1** and **2**.

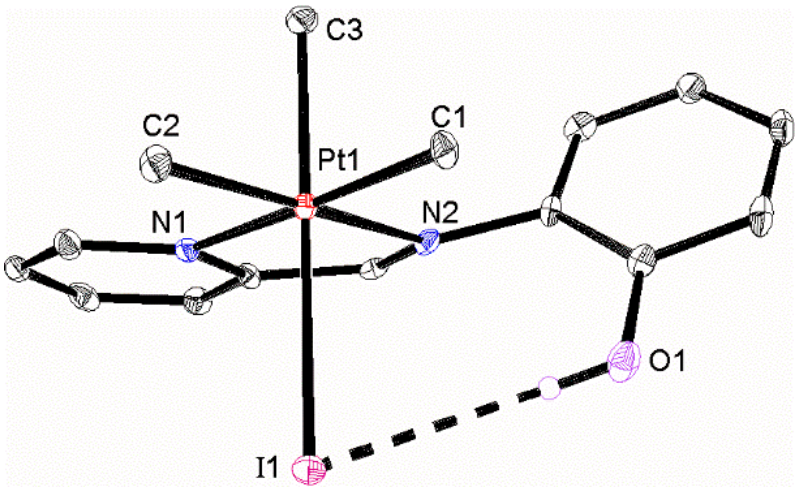

Figure 2. The structure of [PtIMe$_3$(**L2**)], **1**, showing 30% probability ellipsoids. Selected bond distances: Pt(1)C(1) 2.047(5), Pt(1)C(2) 2.050(6), Pt(1)C(3) 2.060(5), Pt(1)N(2) 2.161(5), Pt(1)N(1) 2.164(5), Pt(1)I(1) 2.7803(14), N(2)C(9) 1.284(7) Å. H-bond distance: O(1)I(1) 3.520(4) Å.

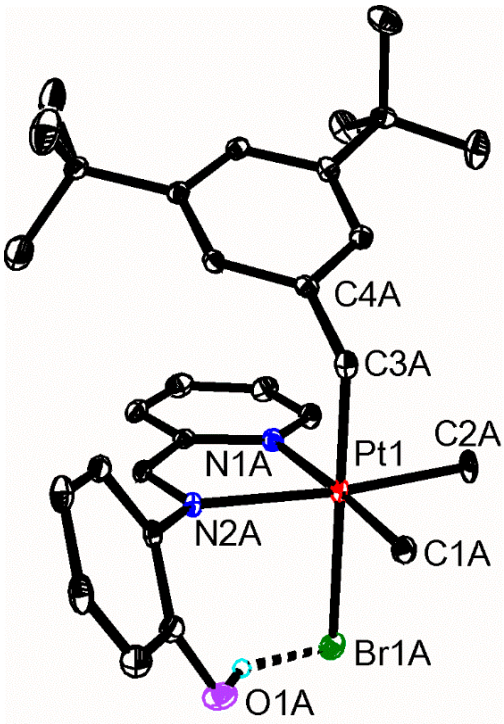

Figure 3. The structure of [PtBrMe$_2$(CH$_2$C$_6$H$_3$-3,5-*t*-Bu$_2$)(**L2**)], **2**, showing 30% probability ellipsoids. Selected bond distances: Pt(1)C(1A) 2.049(4), Pt(1)C(2A) 2.045(4), Pt(1)C(3) 2.075(4), Pt(1)N(2A) 2.186(3), Pt(1)N(1A) 2.156(3), Pt(1)Br(1A) 2.6076(11), N(2)C23A) 1.277(4) Å. H-bond distance: O(1A)Br(1A) 3.188(4) Å.

2.3. Cycloneophyl Complexes with Imine Ligand **L4**

The reaction of [Pt$_2$(CH$_2$CMe$_2$C$_6$H$_4$)$_2$(μ-SMe$_2$)$_2$] [44] with ligand **L4** gave the platinum(II) complex [Pt(CH$_2$CMe$_2$C$_6$H$_4$)(**L4**)], **3**, as a single isomer (Scheme 4a). Complex **3** was isolated as an orange–red solid, this color being characteristic of a platinum(II) complex, and it was stable in dichloromethane solution for at least one day. The corresponding complex of the ligand **L2**, [Pt(CH$_2$CMe$_2$C$_6$H$_4$)(**L2**)], ***H***, was reported previously and has similar spectroscopic properties [38]. The observation of the imine proton in the ^{1}H NMR spectrum of **3** [δ(^{1}H) = 9.58 (s, ^3J(PtH) = 25 Hz)] proves that the imine structure is maintained. Both complexes **3** and ***H*** give very broad resonances for the PtCH$_2$ protons of the cycloneophyl group due to fluxionality. The formation of the OH··Pt hydrogen bond leads to a loss of the effective plane of symmetry and thus to non-equivalence of the PtCH^{A}H^B protons of the cycloneophyl group, and cleavage of the hydrogen bond is required to make them equivalent (Scheme 4b). As seen in variable-temperature NMR studies, the value of the activation energy for fluxionality for **3** was $\Delta G^{\dagger}$ = 60(1) kJ mol^{-1}, compared to the value of $\Delta G^{\dagger}$ = 55(1) kJ mol^{-1} for complex *H* [38]. The difference can be attributed to the greater acidity of L4 compared to L2, leading to a stronger OH··Pt hydrogen bond in 3 than in *H*. However, this nitro group effect is not great enough to cause complete proton transfer to platinum to form a platinum(IV) hydride.

The reaction of complex **3** with methyl iodide gave the platinum(IV) complex [PtIMe(CH$_2$CMe$_2$C$_6$H$_4$)(**L4**)], **4**, as a mixture of two isomers **4a** and **4b** (Scheme 4a), with a ratio **4a**:**4b** of approximately 1:2. When the reaction was monitored by ^{1}H NMR spectroscopy, the first product formed was **4a** and it equilibrated with **4b** over a period of one hour. The methylplatinum resonances were observed at δ 1.81, ^2J(PtH) = 72 Hz, and at δ 1.22, ^2J(PtH) = 72 Hz, for **4a** and **4b**, respectively. Both isomers are chiral and so the methylene protons of the cycloneophyl group appear as AB multiplets. The imine protons were observed at δ 8.84, ^3J(PtH) = 20 Hz, and at δ 9.07, ^3J(PtH) = 18 Hz, for **4a** and **4b**, respectively.

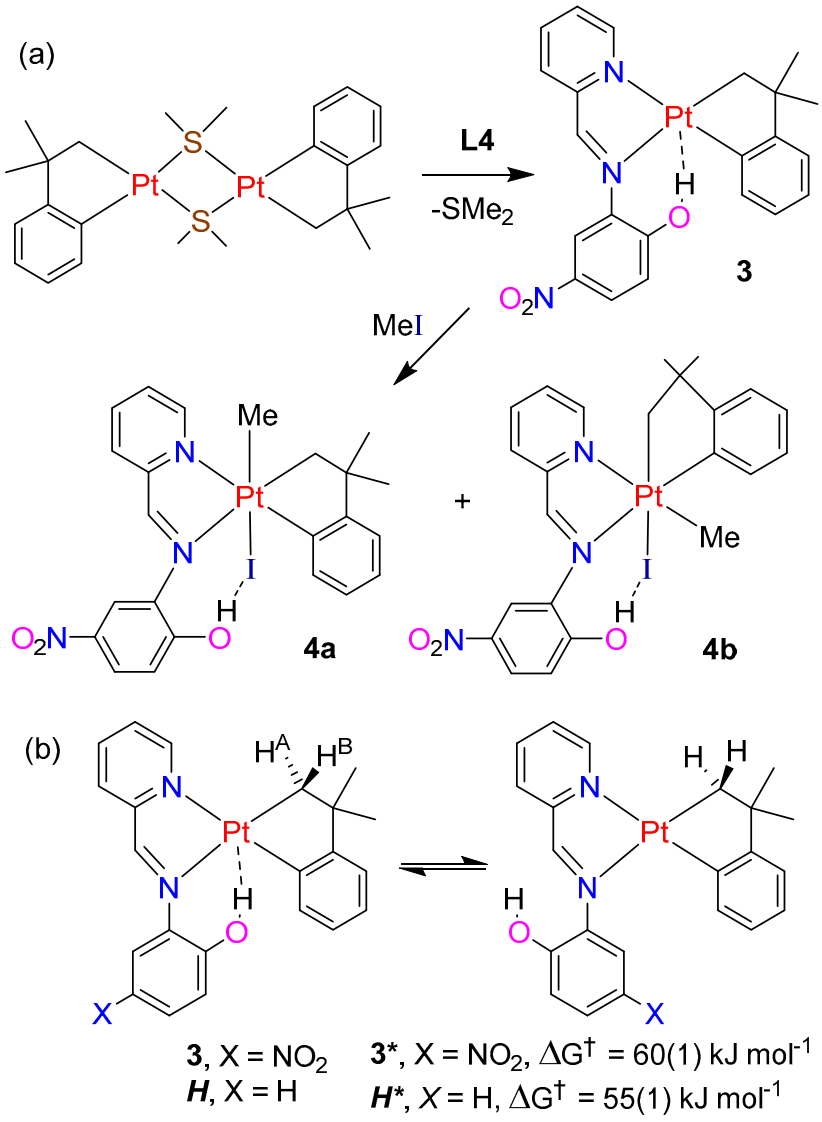

Scheme 4. Cycloneophyl complexes with ligand **L4**; (**a**) synthesis of complexes **3** and **4** and (**b**) fluxionality of complexes **3** and ***H***.

2.4. Cycloneophyl Complexes with Ligand **L3**

The reaction of $[Pt_2(CH_2CMe_2C_6H_4)_2(\mu\text{-}SMe_2)_2]$ with ligand **L3** was more complex and was solvent-dependent. The reaction in acetone solution gave a mixture of five compounds, perhaps isomers, in a ratio of about 10:6:1:1:0.4, characterized in the ^{1}H NMR spectrum of the mixture by the *ortho* pyridyl proton resonance at δ(H6) = 8.77, 9.06, 9.18, 8.88 and 8.92, respectively. The compounds could not be identified by their NMR spectra, but recrystallisation from methanol gave crystals of the major isomer, which was identified as $[Pt(OH)(CH_2CMe_2C_6H_4)(\mathbf{L3\text{-}H})]$, **5**, as the methanol solvate, via X-ray structure determination (Scheme 5, Figures 4 and 5). The formation of complex **5** involves the activation of dioxygen and is analogous to the formation of complex ***F*** (Scheme 2), although in that case it was a different isomer that crystallized [37]. As in related systems, the reaction is likely to involve a shortlived hydroperoxide complex intermediate [21–24,62–64], which might be formed either by the direct reaction of dioxygen with the platinum(II) precursor or by the insertion of dioxygen into a hydridoplatinum(IV) intermediate [24,28,32,62]. In both complexes **5** and ***F***, the deprotonated ligand **L3-H** acts as a *fac*-κ^3-*N*,*N′*,*O* tridentate ligand, a geometry that has not been observed with platinum(IV) complexes of the imine ligand **L4**. In the crystal, complex **5** forms a hydrogen-bonded supramolecular polymeric structure. There are dimer units formed by complementary hydrogen bonding N(2)H··O(2B) and

N(2A)H··O(2) groups, with NH groups as H-bond donors and PtOH groups as acceptors (Figure 5). These dimer units were connected to neighbors by intermolecular hydrogen bonds PtO(2)H··O(Me)H··O(1A)Pt, in which a solvate methanol molecule acts as a hydrogen bond acceptor from the PtOH group of one molecule and as an H-bond donor to the Pt-O group of a deprotonated **L3** ligand of another (Figures 4 and 5).

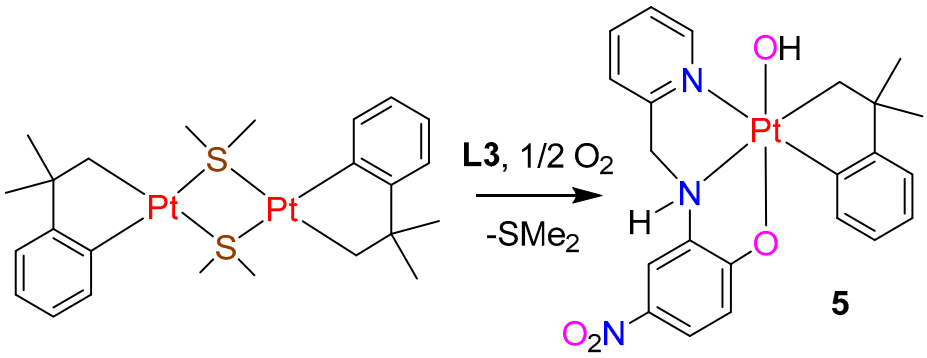

Scheme 5. The formation of complex **5**.

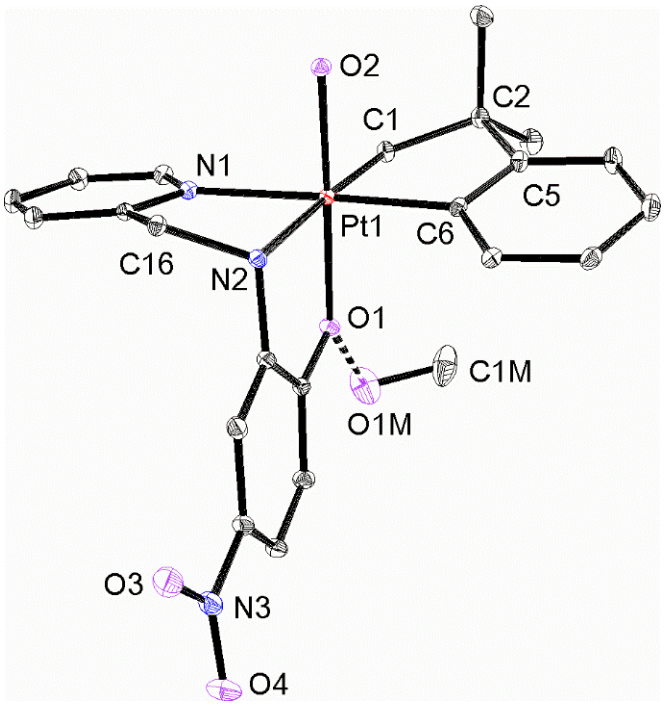

Figure 4. The structure of complex **5**, showing 30% probability ellipsoids. Selected bond distances: Pt(1)C(1) 2.0500(18), Pt(1)C(6) 1.9968(18), Pt(1)N(1) 2.1567(16), Pt(1)N(2) 2.1725(16), Pt(1)O(1) 2.0447(15), Pt(1)O(2) 1.9936(15) Å; C(6)Pt(1)C(1) 81.24(7), N(1)Pt(1)N(2) 78.53(6) °.

The reaction of $[Pt_2(CH_2CMe_2C_6H_4)_2(\mu\text{-}SMe_2)_2]$ with ligand **L3** in CD_2Cl_2 solution, as monitored by ^{1}H NMR spectroscopy under nitrogen, was also complex (Figure 6). After five minutes reaction time, the dimethylsulfide ligands had been displaced to give a mixture of four isomeric platinum(IV) hydride complexes $[PtH(CH_2CMe_2C_6H_4)(\mathbf{L3}\text{-H})]$, **7**. These isomers were initially formed in abundances **7a** (72%), **7b** (21%), **7c** (4%) and **7d** (3%) as determined by the integration of the characteristic PtH resonances for **7a** ($\delta = -18.81$, ^1J(PtH) = 1479 Hz), **7b** ($\delta = -21.23$, ^1J(PtH) = 1449 Hz), **7c** ($\delta = -18.86$, ^1J(PtH) = 1480 Hz) and **7d** ($\delta = -19.42$, ^1J(PtH) = 1434 Hz). After 40 min and after 24 h, these isomers remained but the abundances changed to **7a** (20%), **7b** (60%), **7c** (10%) and **7d** (10%) and to **7a** (10%), **7b** (60%), **7c** (10%) and **7d** (20%), respectively. No further change in isomer ratio occurred,

but slow decomposition occurred over a period of weeks. What is clear from these data is that **7a** and **7b** are the major isomers of kinetic and thermodynamic control, respectively, and that the interconversion of isomers is relatively slow at room temperature. However, it is more challenging to assign the structures of the isomers or to determine the mechanisms of both the initial reaction and the subsequent isomerization steps.

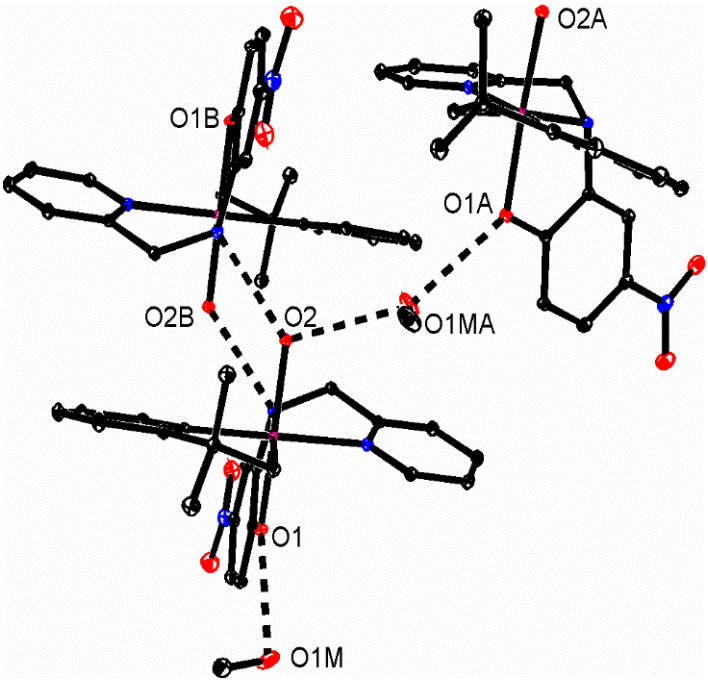

Figure 5. Part of the hydrogen-bonded polymeric structure of complex **5**. H-bond distances: O(1)··O(1M) 2.809(2), O(2)··O(1MA) 2.879(2), O(2)..N(2B) 2,707(2) Å. Equivalent atoms: x, y, z; a, x-½, -y-½, z-½; b, 1-x, 1-y, 1-z.

Some suggestions of likely mechanisms, based on the experimental observations and on DFT calculations (see experimental section for details), are summarized in Schemes 6 and 7. It is likely that the first step is the displacement of the dimethylsulfide ligands from $[Pt_2(CH_2CMe_2C_6H_4)_2(\mu\text{-}SMe_2)_2]$ by the ligand **L3** to give $[Pt(CH_2CMe_2C_6H_4)(\mathbf{L3})]$, which may exist as isomers **6** and **6a** (Scheme 6). In most analogous complexes (e.g., complexes **3** and ***H***), the isomer with the aryl group *trans* to the pyridyl group is preferred, but the presence of strong OH··Pt hydrogen bond leads to the distortion of the square planar stereochemistry so that **6** and **6a** are calculated to have the same energy. Concerted oxidative addition of the O-H bond to platinum(II) might then give isomers **7a**–**7d**, with **7a** predicted to be the kinetically favored product (Scheme 6). Complexes **7a**–**7c** are predicted to be accessible directly from **6** or **6a**, but the activation energy for the formation of **7d** from **6** is predicted to be too high to allow the formation of **7d** at room temperature (Scheme 6). A subsequent pairwise exchange between hydride and alkyl or aryl groups can lead to subsequent isomerization steps, as illustrated in Scheme 7 [37]. The lowest energy isomers are predicted to be **7b** and **7d**, with CH_2 *trans* to O, while the highest energy isomers are **7e** and **7f**, with hydride *trans* to O. These isomers **7e** and **7f** were not observed, and they are expected to be present in only very low concentration at equilibrium. There are also potential isomers with hydride *trans* to CH_2 or C_6H_4, but these are predicted to lie at a higher energy and are not accessible.

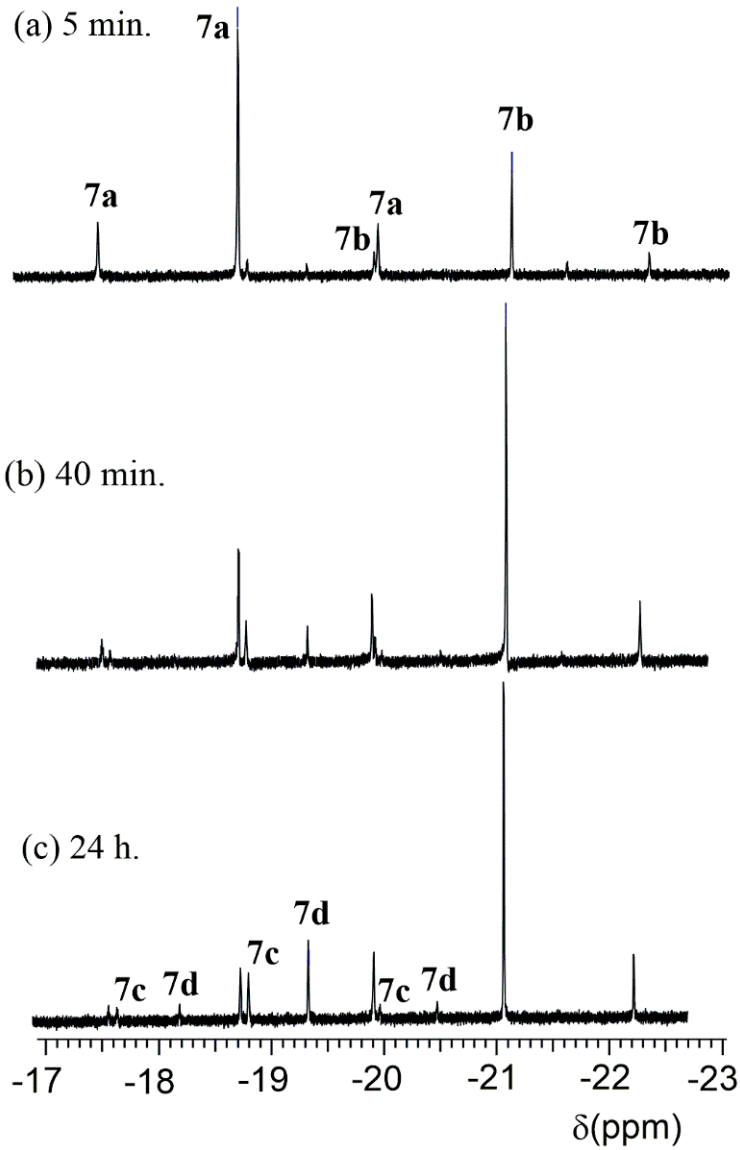

Figure 6. ^{1}H NMR spectra in the PtH region for the reaction of $[Pt_2(CH_2CMe_2C_6H_4)_2(\mu\text{-}SMe_2)_2]$ with ligand **L3** in CD_2Cl_2 solution at different times. Subfigures (**a**), (**b**), (**c**) after 5 min, 40 min, 24 h, respectively.

2.5. A Comparison of Complexes with **L3** and **L4**

In complexes such as **7**, in Schemes 6 and 7, the hydride and carbon donors have a strong preference for the *fac* stereochemistry and so, to accommodate this, the deprotonated ligand **L3-H** must also take the *fac* stereochemistry. This is easily achieved with the amine ligand **L3** but not with the imine ligand **L4**, in which the planar imine unit leads to strain in the *fac*-PtN,N′,O coordination mode. In stable organoplatinum(IV) complexes with the imine ligands **L2** and **L4**, there is typically a halide ligand and the intact phenol unit forms a hydrogen bond OH··XPt, as in complexes **1**, **2** and **4** (Schemes 3 and 4). On the other hand, the deprotonated imine ligands are better suited to act as tridentate pincer ligands in platinum(II) complexes. These trends are supported by DFT calculations illustrated in Figure 7. The intramolecular oxidative addition of the O-H bond of complex **6** to give isomers of **7** (illustrated by **7c** in Figure 7, see also Scheme 7) is favorable, but a similar reaction of the imine complex **3** is unfavorable, in agreement with the observation that the hydridoplatinum(IV) complex $[PtH(CH_2CMe_2C_6H_4)(\mathbf{L4\text{-}H})]$, ***J***, or its isomers, is not observed. The potential reductive elimination from complex **7** might give either $[Pt(CH_2CMe_2Ph)(\mathbf{L3\text{-}H})]$ or $[Pt(C_6H_4\text{-}2\text{-}t\text{-}Bu)(\mathbf{L3\text{-}H})]$, ***I***, by a combination of the hydride

with sp^2 or sp^3 carbon donors, respectively. Complex ***I*** is calculated to be more stable, but its formation from **7** is still not favored, consistent with the observation that isomers of **7** are stable at room temperature. In contrast, the reductive elimination of ***J*** to give [Pt(C_6H_4-2-*t*-Bu)(**L3-H**)], ***K***, is calculated to be strongly favored as the strained *fac* stereochemistry of **L3-H** in ***J*** is replaced by the planar pincer stereochemistry in ***K***. Although ***K*** is the most stable isomer, it is not formed at room temperature due to the high activation energy needed to reach the likely intermediate ***J*** (Figure 7).

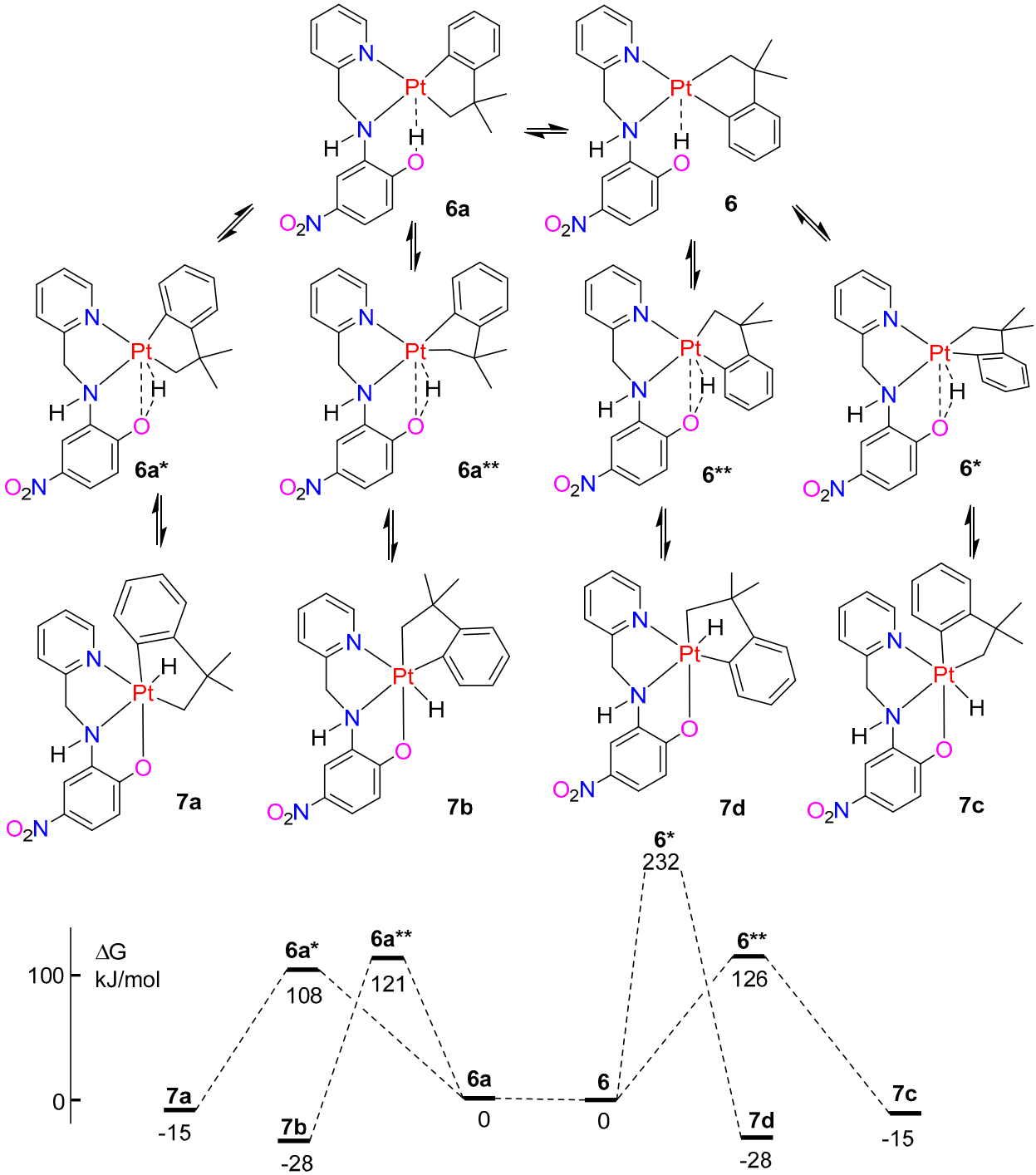

Scheme 6. A possible route for the formation of isomers of complex **7**, and their calculated relative energies. The signs * or ** indicate a transition state structure.

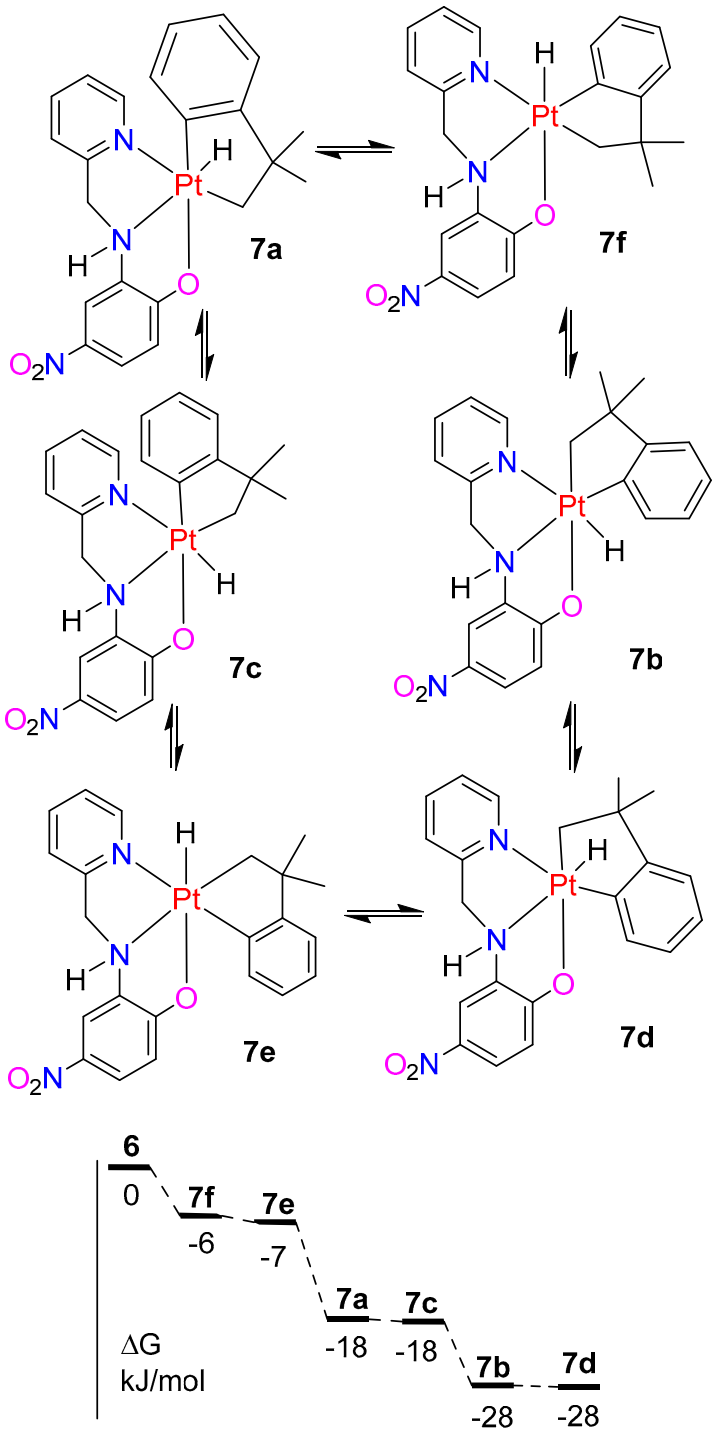

Scheme 7. A possible sequence of isomerization of isomers of complex **7** from the kinetic product **7a**, and the calculated relative energies of the isomers.

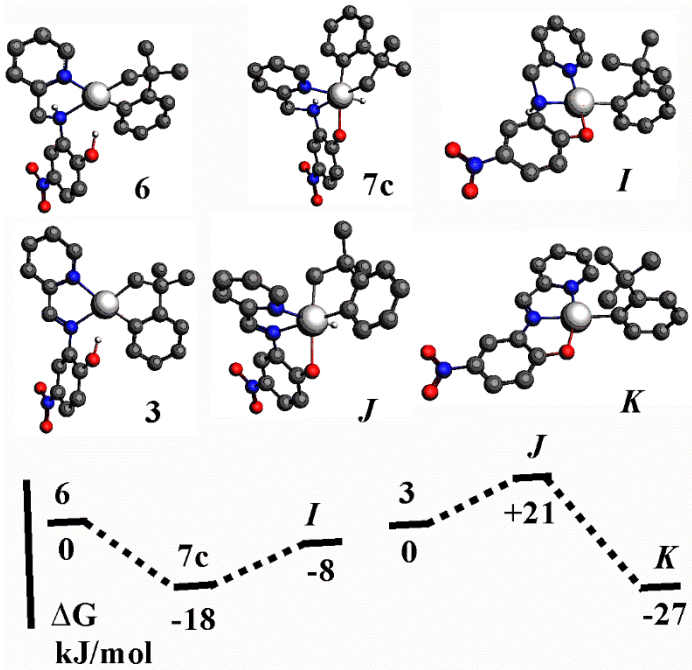

Figure 7. Calculated structures and relative energies for complexes [Pt($CH_2CMe_2C_6H_4$)**L**], **6** and **3**, [PtH($CH_2CMe_2C_6H_4$)(**L-H**)], **7c** and ***J***, and [Pt(2-C_6H_4-*t*-Bu)(**L-H**)], ***I*** and ***K***, with **L** = **L3** or **L4**.

3. Materials and Methods

The compounds [Pt_2Me_4(μ-SMe_2)$_2$] [65], [Pt_2($CH_2CMe_2C_6H_4$)(μ-SMe_2)$_2$] [44], and ligands **L1**–**L4** [34,37,38,55] were prepared using the literature methods. NMR spectra were recorded using a Varian Inova 400 NMR or a Varian Inova 600 NMR spectrometer at room temperature and were reported using the labeling system of Scheme 8. Assignments were assisted by recording the COSY spectra.

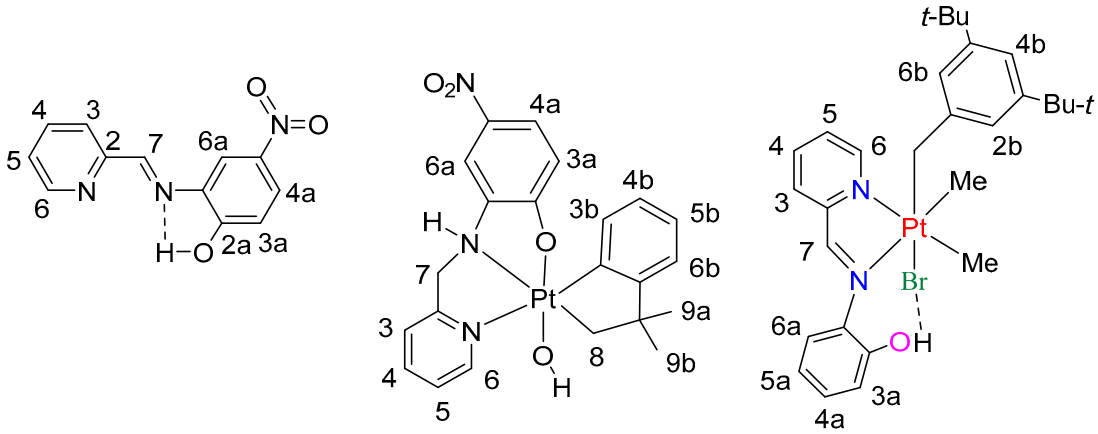

Scheme 8. NMR labeling scheme.

Structure determinations.

Typically, a sample single crystal was mounted on a Mitegen polyimide micromount with a small amount of Paratone N oil. All X-ray measurements were made by using a Bruker Kappa Axis Apex2 diffractometer at a temperature of 110 K. The data collection strategy was a number of ω and φ scans and frame integration was performed using SAINT [66]. The resulting raw data were scaled and absorption corrected using a multi-scan averaging of symmetry-equivalent data using SADABS [67]. The structures were solved by using a dual space methodology using the SHELXT program [68]. The hydrogen atoms were introduced at idealized positions and were allowed to ride on the parent atom.

The structures were refined using the SHELXL program from the SHELX-2014 suite of crystallographic software [69]. Details of individual structure determinations are given in the cif files (CCDC 2243128-2243130).

DFT calculations.

The DFT calculations were carried out using the NEB (nudged elastic band) method for finding the minimum energy reaction paths because this method can roughly track the reaction coordinate and gives good insight into the reaction mechanism [70,71]. The BLYP functional was used, with double-zeta basis set and first-order scalar relativistic corrections [72]. The solvent effect of dichloromethane was modeled by using COSMO [73], all as implemented in ADF-2020 [74]. Details of the calculated ground state and transition state structures are given in the Supporting Information.

C_5H_4N-2-CH=NC_6H_3-2-OH-5-NO_2, L4.

To a solution of C_6H_3-1-NH_2-2-OH-5-NO_2 (0.50 g, 3.24 mmol) in dry CH_2Cl_2 (5 mL) C_5H_4N-2-CHO (0.31 mL, 3.24 mmol) was added. The mixture was stirred for 2 h, then the volume was reduced, and the product was separated by filtration as a white solid, which was washed with pentane and dried under vacuum. Yield 0.64 g, 81%. NMR in CD_2Cl_2: $\delta(^1H)$ = 8.96 (s, 1H, H7); 8.75 (d, 1H, ^3J(HH) = 5 Hz, H6); 8.37 (s, 1H, H6a); 8.24 (d, 1H, ^3J(HH) = 7 Hz, H4a); 8.17 (d, 1H, ^3J(HH) = 7 Hz, H3); 7.88 (t, 1H, ^3J(HH) = 7 Hz, H4); 7.46 (dd, 1H, ^3J(HH) = 5 Hz, 7 Hz, H5); 7.12 (d, 1H, ^3J(HH) = 7 Hz, H3a). EI-MS: Found, m/z = 243.05; Calc. for $C_{12}H_9N_3O_3$, m/z = 243.06. NMR of **L5** in CD_3OD: $\delta(^1H)$ = 8.59 (d, 1H, ^3J(HH) = 5 Hz, H6); 7.89 (t, 1H, ^3J(HH) = 7 Hz, H4); 7.75 (s, 1H, H6a); 7.66 (d, 1H, ^3J(HH) = 7 Hz, H3); 7.58 (d, 1H, ^3J(HH) = 7 Hz, H4a); 7.39 (dd, 1H, ^3J(HH) = 5 Hz, 7 Hz, H5); 6.80 (d, 1H, ^3J(HH) = 7 Hz, H3a); 5.86 (s, 1H, H7).

[$PtIMe_3$(L2)], 1.

To a stirred solution of [$PtMe_2$(**L2**)](0.44 g, 0.1 mmol) in acetone (3 mL), MeI (20 µL, 0.3 mmol) was added. The solution was stirred at room temperature for 1 h. The color changed from deep purple to colorless with precipitation of a pale yellow solid product, which was collected by filtration, washed with pentane (3x 3 mL) and dried under vacuum (yield 0.53g, 89%). It was purified by crystallization from dichloromethane/ether. NMR in $CDCl_3$: $\delta(^1H)$ = 9.01 (d, 1H, J_{HH} = 6 Hz, $^3J_{PtH}$ = 18 Hz, H6), 8.81 (s, 1H, $^3J_{PtH}$ = 25 Hz, CH=N), 8.12 (t, 1H, J_{HH} = 8 Hz, H4), 8.06 (d, 1H, J_{HH} = 8 Hz, H3), 7.72 (dd, 1H, J_{HH} = 6 Hz, 8 Hz, H5), 7.25 (t, 1H, J_{HH} = 8 Hz, H5a), 7.06 (d, 2H, J_{HH} = 8 Hz, H6a), 6.94 (t, 1H, J_{HH} = 9 Hz, H4a), 6.88 (d, 1H, J_{HH} = 8 Hz, H3a), 1.56 (s, 3H, $^3J_{PtH}$ = 72 Hz, PtMe), 1.17 (s, 3H, $^3J_{PtH}$ = 72 Hz, PtMe), 0.60 (s, 3H, $^3J_{PtH}$ = 73 Hz, PtMe).

[$PtBrMe_2$($CH_2C_6H_3$-3,5-*t*-Bu_2)(L2)], 2.

This was prepared similarly but using 3,5-di-*t*-butylbenzyl bromide (yield 75%). It was purified via crystallization from chloroform/ether. NMR in $CDCl_3$: $\delta(^1H)$ = 8.70 (s, 1H, $^3J_{PtH}$ = 27 Hz, CH=N), 8.39 (d, 1H, J_{HH} = 6 Hz, $^3J_{PtH}$ = 16 Hz, H6), 7.84 (t, 1H, J_{HH} = 8 Hz, H4), 7.73 (d, 1H, J_{HH} = 8 Hz, H3), 7.31 (dd, 1H, J_{HH} = 6 Hz, 8 Hz, H5), 7.23 (t, 1H, J_{HH} = 8 Hz, H4a), 7.22(s, 2H, H2b,H6b), 7.03 (d, 1H, J_{HH} = 8 Hz, H6a), 6.88 (t, 1H, J_{HH} = 8 Hz, H5a), 6.87 (t, 1H, J_{HH} = 8 Hz, H4a), 6.69 (d, 1H, J_{HH} = 8 Hz, H3a), 6.57 (s, 1H, H4b), 2.75(d, 1H, J_{HH} = 8 Hz, $^3J_{PtH}$ = 86 Hz, CH^A), 2.73 (d, 1H, J_{HH} = 8 Hz, $^3J_{PtH}$ = 72 Hz, CH^B), 1.60 (s, 3H, $^3J_{PtH}$ = 72 Hz, PtMe), 1.17 (s, 3H, $^3J_{PtH}$ = 72 Hz, PtMe), 1.2 (s, 18H, *t*Bu),

[Pt($CH_2CMe_2C_6H_4$)(C_5H_4N-2-CH=NC_6H_3-2-OH-5-NO_2)], 3.

A mixture of [$Pt_2(CH_2CMe_2C_6H_4)_2(\mu\text{-}SMe_2)_2$] (80 mg, 0.103 mmol) and **L4** (56 mg, 0.230 mmol) in ether (5 mL) was stirred for 1 day to give an orange–red suspension. This was separated using filtration, washed with ether (2 mL) and pentane (2 mL) and dried under vacuum (yield 74 mg, 46%). It was purified via crystallization from acetone/ether. NMR in CD_2Cl_2: $\delta(^1H)$ = 9.58 (s, 1H, ^3J(PtH) = 25 Hz, H7); 9.25 (d, 1H, ^3J(HH) = 5 Hz, ^3J(PtH) = 30 Hz, H6); 8.30 (s, 1H, H6a); 8.20-8.24 (m, 2H, H4, H4a); 8.07 (d, 1H, ^3J(HH) = 7 Hz, H3); 7.80 (dd, 1H, ^3J(HH) = 5 Hz, 7 Hz, H5); 7.03 (d, 1H, ^3J(HH) = 7 Hz, H3a); 6.84 (m, 2H, H5b, H6b), 6.52 (dd, 1H, ^3J(HH) = 7 Hz, 9 Hz, H4b), 6.49 (d, 1H, ^3J(HH) = 7 Hz, ^3J(PtH) = 48 Hz, H3b); 3.51 (br, 1H, ^2J(PtH) = 100 Hz, H8); 2.61 (br, 1H, ^2J(PtH) = 102 Hz, H8′); 1.34 (s, 6H, H9).

Coalescence of H8, H8′ resonances; Δν = 360 Hz, T_c = 318K, $\Delta G^{\dagger}$ = 60(1) kJ mol^{-1}. ESI-MS: Found, m/z = 593.12; Calc. for $C_{12}H_{21}N_3O_3Pt{+}Na^+$, m/z = 593.11.

[PtIMe($CH_2CMe_2C_6H_4$)(C_5H_4N-2-CH=NC_6H_3-2-OH-5-NO_2)], 4.

A mixture of [$Pt_2(CH_2CMe_2C_6H_4)_2(\mu\text{-}SMe_2)_2$] (80 mg, 0.103 mmol) and **L4** (56 mg, 0.230 mmol) in ether (5 mL) was stirred for 1 day to give an orange–red suspension, and then MeI (0.2 mL) was added and the mixture was stirred for 9 h to give a yellow solution. The solvent was evaporated and the product was crystallized from acetone/pentane (yield 95 mg, 65%). NMR in CD_2Cl_2: major isomer, **4b**, δ(^{1}H) = 9.07 (s, 1H, ^3J(PtH) = 18 Hz, H7); 8.40 (d, 1H, ^3J(HH) = 5 Hz, ^3J(PtH) = 14 Hz, H6); 8.28 (m, 1H, H4a); 8.22 (m, 1H, H4); 8.20 (d, 1H, ^3J(HH) = 7 Hz, H3); 7.96 (s, 1H, H6a); 7.62 (dd, 1H, ^3J(HH) = 5 Hz, 7 Hz, H5); 7.27 (d, 1H, ^3J(HH) = 7 Hz, H3a); 7.05 (m, 1H, H5b); 6.96 (dd, 1H, ^3J(HH) = 7 Hz, 9 Hz, H4b); 6.82 (m, 1H, H6b); 6.69 (d, 1H, ^3J(HH) = 7 Hz, H3b); 2.56 (d, 1H, ^2J(HH) = 12 Hz, ^2J(PtH) = 92 Hz, H8); 1.97 (d, 1H, ^2J(HH) = 12 Hz, ^2J(PtH) = 100 Hz, H8′); 1.22 (s, ^2J(PtH) = 72 Hz, MePt); 1.19 (s, 3H, H9); 0.83 (s, 3H, H9′): minor isomer, **4a**, resolved resonances only, δ(^{1}H) = 9.23 (d, 1H, ^3J(HH) = 5 Hz, ^3J(PtH) = 14 Hz, H6); 8.84 (s, 1H, ^3J(PtH) = 20 Hz, H7); 8.23 (s, 1H, H6a); 8.14 (m, 1H, H4a); 7.21 (d, 1H, ^3J(HH) = 7 Hz, H3a); 2.92 (d, 1H, ^2J(HH) = 12 Hz, ^2J(PtH) = 68 Hz, H8); 2.67 (d, 1H, ^2J(HH) = 12 Hz, ^2J(PtH) = 100 Hz, H8′); 1.81 (s, ^2J(PtH) = 72 Hz, MePt); 1.11 (s, 3H, H9); 0.55 (s, 3H, H9′). ESI-MS: Found, m/z = 735.05; Calc. for $C_{23}H_{24}IN_3O_3Pt{+}Na^+$, m/z = 735.04.

[Pt(OH)($CH_2CMe_2C_6H_4$)(C_5H_4N-2-CH_2-NHC_6H_3-2-O-5-NO_2)], 5.

A mixture of [$Pt_2(CH_2CMe_2C_6H_4)_2(\mu\text{-}SMe_2)_2$] (84 mg, 0.108 mmol) and **L3** (53 mg, 0.216 mmol) in acetone (5 mL) was stirred for 1 day to give a yellow/orange suspension. The solvent volume was reduced under vacuum and n-pentane (5 mL) was added. The solid product was separated using filtration and recrystallized from MeOH (yield: 76 mg, 60%). The ^{1}H NMR spectrum indicated the presence of 5 isomers in approximate ratio 10:6:1:1:0.4. NMR in CD_3OD: isomer 1, δ(^{1}H) = 8.77 [d, 1H, ^3J(HH) = 6 Hz, H6], 8.31 [s, 1H, H6a], 8.11 [t, 1H, ^3J(HH) = 8 Hz, H4], 8.02 [d, 1H, ^3J(HH) = 9 Hz, H4a], 7.78 [d, 1H, ^3J (HH) = 8 Hz, H3], 7.64 [dd, 1H, ^3J(HH) = 6 Hz, 8 Hz, H5], 6.82 [t, 1H, ^3J(HH) = 8 Hz, H5b], 6.75 [d, 1H, ^3J(HH) = 8 Hz, H6b], 6.68 [d, 1H, ^3J(HH) = 9 Hz, H3a], 6.48 [t, 1H, ^3J(HH) = 8 Hz, H4b], 6.43 [d, 1H, ^3J(HH) = 8 Hz, H3b], 5.25 [d, 1H, ^2J(HH) = 16 Hz, H7], 4.78 [d, 1H, ^2J(HH) = 16 Hz, H7′], 3.89 [d, 1H, ^2J(PtH) = 77 Hz, ^2J(HH) = 7 Hz, H8], 3.55 [d, 1H, ^2J(PtH) = 77 Hz, ^2J(HH) = 7 Hz, H8′], 1.36 [s, 6H, H9, H9′]; isomer 2, δ(^{1}H) = 9.06 [d, 1H, ^3J(HH) = 6 Hz, H6], 8.16 [s, 1H, H6a], 8.10 [t, 1H, ^3J(HH) = 8 Hz, H4], 7.89 [d, 1H, ^3J(HH) = 9 Hz, H4a], 7.78 [d, 1H, ^3J (HH) = 8 Hz, H3], 7.73 [dd, 1H, ^3J(HH) = 6 Hz, 8 Hz, H5], 6.94 [t, 1H, ^3J(HH) = 8 Hz, H5b], 6.84 [d, 1H, ^3J(HH) = 8 Hz, H6b], 6.68 [t, 1H, ^3J(HH) = 8 Hz, H4b], 6.56 [d, 1H, ^3J(HH) = 9 Hz, H3a], 6.33 [d, 1H, ^3J(HH) = 8 Hz, H3b], 5.24 [d, 1H, ^2J(HH) = 16 Hz, H7], 4.52 [d, 1H, ^2J(HH) = 16 Hz, H7′], 2.97 [d, 1H, ^2J(PtH) = 77 Hz, ^2J(HH) = 7 Hz, H8], 3.07 [d, 1H, ^2J(PtH) = 77 Hz, ^2J(HH) = 7 Hz, H8′], 1.35 [s, 6H, H9, H9′]. Three further compounds were present in the initial product mixture, characterized by doublet resonances at δ(^{1}H) = 9.18 [d, ^3J(HH) = 6 Hz, H6], 8.88 [d, ^3J(HH) = 6 Hz, H6], 8.92 [d, ^3J(HH) = 6 Hz, H6], but complete assignment was not possible.

[Pt(H)($CH_2CMe_2C_6H_4$)(C_5H_4N-2-CH_2-NHC_6H_3-2-O-5-NO_2)], 7.

A mixture of [$Pt_2(CH_2CMe_2C_6H_4)_2(\mu\text{-}SMe_2)_2$] (39 mg, 0.05 mmol) and **L3** (25 mg, 0.12 mmol) was dissolved in CD_2Cl_2 (0.5 mL) in an NMR tube. ^{1}H NMR spectra were recorded after 5 min, 40 min, 24 h and 48 h. After 5 min, the major compound was **7a**: NMR in CD_2Cl_2: δ(^{1}H) = 8.94 [d, 1H, ^3J(HH) = 6 Hz, H6], 8.18 [s, 1H, H6a], 7.96 [t, 1H, ^3J(HH) = 8 Hz, H4], 7.84 [d, 1H, ^3J(HH) = 9 Hz, H4a], 7.53 [d, 1H, ^3J (HH) = 8 Hz, H3], 7.47 [dd, 1H, ^3J(HH) = 6 Hz, 8 Hz, H5], 6.96 [t, 1H, ^3J(HH) = 8 Hz, H5b], 6.84 [d, 1H, ^3J(HH) = 8 Hz, H6b], 6.65 [t, 1H, ^3J(HH) = 8 Hz, H4b], 6.53 [d, 1H, ^3J(HH) = 9 Hz, H3a], 6.31 [d, 1H, ^3J(HH) = 8 Hz, H3b], 5.00 [d, 1H, ^2J(HH) = 15 Hz, H7], 4.66 [d, 1H, ^2J(HH) = 15 Hz, H7′], 2.51 [d, 1H, ^2J(HH) = 7 Hz, H8], 2.40 [d, 1H, ^2J(HH) = 7 Hz, H8′], 1.33, 1.18 [each s, 3H, H9, H9′], −18.81 [s, 1H, ^1J(PtH) = 1479 Hz, PtH]. After 40 min, the major compound was **7b**: NMR in CD_2Cl_2: δ(^{1}H) = 8.68 [d, 1H, ^3J(HH) = 6 Hz, H6], 8.34 [s, 1H, H6a], 7.88 [t, 1H, ^3J(HH) = 8 Hz, H4], 7.79 [d, 1H, ^3J(HH) = 9 Hz, H4a], 7.40–7.45

[m, 2H, H3,H5], 6.96 [t, 1H, ^3J(HH) = 8 Hz, H5b], 6.87 [d, 1H, ^3J(HH) = 8 Hz, H6b], 6.68 [t, 1H, ^3J(HH) = 8 Hz, H4b], 6.36 [d, 1H, ^3J(HH) = 9 Hz, H3a], 6.19 [d, 1H, ^3J(HH) = 8 Hz, H3b], 4.90 [d, 1H, ^2J(HH) = 15 Hz, H7], 4.87 [d, 1H, ^2J(HH) = 15 Hz, H7′], 2.48 [d, 1H, ^2J(HH) = 7 Hz, H8], 2.02 [d, 1H, ^2J(HH) = 7 Hz, H8′], 1.45, 1.29 [each s, 3H, H9, H9′], −21.23 [s, 1H, ^1J(PtH) = 1449 Hz, PtH]. The minor compounds were characterized only by the hydride resonances: **7c** [δ(PtH) = −18.86, ^1J(PtH) = 1480 Hz), and **7d** [δ(PtH) = −19.42, ^1J(PtH) = 1434 Hz].

4. Conclusions

The results presented above allow two main conclusions to be drawn:

1. The nitro group enhances the acidity of the phenol unit in ligands **L3** and **L4**. This is most apparent by comparing the reactions of **L1** and **L3** with [$Pt_2(CH_2CMe_2C_6H_4)_2(\mu$-$SMe_2)_2$] to give either the platinum(II) complex, ***G***, (Scheme 2) or the hydridoplatinum(IV) complex **7** (as a mixture of isomers, Schemes 6 and 7). The difference is less marked in the reactions of **L2** and **L4** with [$Pt_2(CH_2CMe_2C_6H_4)_2(\mu$-$SMe_2)_2$]. These both give the platinum(II) complex, ***H*** (Scheme 2) or **3** (Scheme 4), but there is evidence that the OH··Pt hydrogen bond is stronger in **3** than in ***H***.
2. The platinum(IV) oxidation state is more easily attained with the amine ligand **L3** than with the imine ligand **L4** (Figure 7, compare Schemes 2 and 4).

In summary, the two simple ligand modifications of switching amine and imine centers or replacing a hydrogen by a nitro substituent are shown to have important effects on the reactivity of the organoplatinum complexes of ligands **L1**–**L4**. Such ligand design principles can be expected to influence the design of future catalysts for selective alkane oxidation reactions.

Supplementary Materials: The following supporting information can be downloaded at: https://www.mdpi.com/article/10.3390/inorganics12010032/s1, Figure S1: ^{1}H NMR spectrum of ligand **L2**; Figure S2: ^{1}H NMR spectrum of complex **1**; Figure S3: ^{1}H NMR spectrum of complex **2**; Figure S4: ^{1}H NMR spectra in the PtH region during formation and isomerization of complexes **7a**–**7d**. Table S1: Summary of Crystal Data for complex 1; Table S2: Summary of Crystal Data for complex 2; Table S3: Summary of Crystal Data for complex 5; Table S4. Selected Bond Lengths and Angles for Complex 1; Table S5. Selected Bond Lengths and Angles for Complex 2; Table S6. Selected Bond Lengths and Angles for Complex 5. CCDC 2243128-2243130 contain the supplementary crystallographic data for three complexes. These data can be obtained free of charge via http://www.ccdc.cam.ac.uk/conts/retrieving.html, accessed on 19 January 2023, or from the Cambridge Crystallographic Data Centre, 12 Union Road, Cambridge CB2 1EZ, UK; fax: (+44) 1223-336-033; or e-mail: deposit@ccdc.cam.ac.uk.

Author Contributions: Conceptualization, A.A.-A., M.E.M. and R.J.P.; methodology, P.D.B.; investigation, A.A.-A., M.E.M. and P.D.B.; writing—original draft preparation, A.A.-A., M.E.M. and P.D.B.; writing—review and editing, R.J.P. All authors have read and agreed to the published version of the manuscript.

Funding: This research was funded by NSERC (Canada).

Data Availability Statement: The data presented in this study are available in this article and Supplementary Material.

Conflicts of Interest: The authors declare no conflicts of interest. The funders had no role in the design of the study; in the collection, analyses, or interpretation of data; in the writing of the manuscript; or in the decision to publish the results.

References

1. Manna, S.; Kong, W.J.; Backvall, J.E. Metal-catalyzed biomimetic aerobic oxidation of organic substrates. *Adv. Catal.* **2021**, *69*, 1–57.
2. Chakrabarty, S.; Wang, Y.; Perkins, J.C.; Narayan, A.R.H. Scalable biocatalytic C-H oxyfunctionalization reactions. *Chem. Soc. Rev.* **2020**, *49*, 8137–8155. [CrossRef] [PubMed]
3. Guillemard, L.; Kaplaneris, N.; Ackermann, L.; Johansson, M.J. Late-stage C-H functionalization offers new opportunities in drug discovery. *Nat. Rev. Chem.* **2021**, *5*, 522–545. [CrossRef] [PubMed]

4. Liang, Y.; Wei, J.; Qiu, X.; Jiao, N. Homogeneous Oxygenase Catalysis. *Chem. Rev.* **2018**, *118*, 4912–4945. [CrossRef]
5. Huang, X.; Groves, J.T. Oxygen Activation and Radical Transformations in Heme Proteins and Metalloporphyrins. *Chem. Rev.* **2018**, *118*, 2491–2553. [CrossRef]
6. Groves, J.T.; Feng, L.; Austin, R.N. Structure and Function of Alkane Monooxygenase (AlkB). *Acc. Chem. Res.* **2023**, *56*, 3665–3675. [CrossRef]
7. Liu, Y.G.; You, T.; Wang, H.-X.; Tang, Z.; Zhou, C.-Y.; Che, C.-M. Iron- and cobalt-catalyzed C(sp3)-H bond functionalization reactions and their application in organic synthesis. *Chem. Soc. Rev.* **2020**, *49*, 5310–5358. [CrossRef]
8. Tang, C.; Qiu, X.; Cheng, Z.; Jiao, N. Molecular oxygen-mediated oxygenation reactions involving radicals. *Chem. Soc. Rev.* **2021**, *50*, 8067–8101. [CrossRef]
9. Fukuzumi, S.; Cho, K.-B.; Lee, Y.-M.; Hong, S.; Nam, W. Mechanistic dichotomies in redox reactions of mononuclear metal-oxygen intermediates. *Chem. Soc. Rev.* **2020**, *49*, 8988–9027. [CrossRef]
10. Warren, J.J.; Tronic, T.A.; Mayer, J.M. Thermochemistry of Proton-Coupled Electron Transfer Reagents and its Implications. *Chem. Rev.* **2010**, *110*, 6961–7001. [CrossRef]
11. Munz, D.; Strassner, T. Alkane C-H Functionalization and Oxidation with Molecular Oxygen. *Inorg. Chem.* **2015**, *54*, 5043–5052. [CrossRef] [PubMed]
12. Etim, U.J.; Bai, P.; Gazit, O.M.; Zhong, Z. Low-Temperature Heterogeneous Oxidation Catalysis and Molecular Oxygen Activation. *Catal. Rev. Sci. Eng.* **2023**, *65*, 239–425. [CrossRef]
13. Machan, C.W. Advances in the Molecular Catalysis of Dioxygen Reduction. *ACS Catal.* **2020**, *10*, 2640–2655. [CrossRef]
14. Gunsalus, N.J.; Koppaka, A.; Park, S.H.; Bischof, S.M.; Hashiguchi, B.G.; Periana, R.A. Homogeneous Functionalization of Methane. *Chem. Rev.* **2017**, *117*, 8521–8573. [CrossRef]
15. Schultz, J.W.; Rath, N.P.; Mirica, L.M. Improved Oxidative C-C Bond Formation Reactivity of High-Valent Pd Complexes Supported by a Pseudo-Tridentate Ligand. *Inorg. Chem.* **2020**, *59*, 11782–11792. [CrossRef]
16. Cha, J.M.; Lee, E.S.; Yandulov, D.V. Mechanistic Studies for Pd(II)(O_2) Reduction Generating Pd(0) and H_2O: Formation of $Pd(OH)_2$ as a Key Intermediate. *Inorg. Chem.* **2022**, *61*, 14544–14552. [CrossRef] [PubMed]
17. Wang, D.; Weinstein, A.B.; White, P.B.; Stahl, S.S. Ligand-Promoted Palladium-Catalyzed Aerobic Oxidation Reactions. *Chem. Rev.* **2018**, *118*, 2636–2679. [CrossRef] [PubMed]
18. Sberegaeva, A.V.; Zavalij, P.Y.; Vedernikov, A.N. Oxidation of a Monomethylpalladium(II) Complex with O_2 in Water: Tuning Reaction Selectivity to Form Ethane, Methanol, or Methylhydroperoxide. *J. Am. Chem. Soc.* **2016**, *138*, 1446–1455. [CrossRef]
19. Desnoyer, A.N.; Love, J.A. Recent advances in well-defined, late transition metal complexes that make and/or break C-N, C-O and C-S bonds. *Chem. Soc. Rev.* **2017**, *46*, 197–238. [CrossRef]
20. Boisvert, L.; Goldberg, K.I. Reactions of Late Transition Metal Complexes with Molecular Oxygen. *Acc. Chem. Res.* **2012**, *45*, 899–910. [CrossRef]
21. Labinger, J.A. Platinum-Catalyzed C-H Functionalization. *Chem. Rev.* **2017**, *117*, 8483–8496. [CrossRef] [PubMed]
22. Prantner, J.D.; Kaminsky, W.; Goldberg, K.I. Methylplatinum(II) and Molecular Oxygen: Oxidation to Methylplatinum(IV) in Competition with Methyl Group Transfer to Form Dimethylplatinum(IV). *Organometallics* **2014**, *33*, 3227–3230. [CrossRef]
23. Sberegaeva, A.V.; Watts, D.; Vedernikov, A.N. Oxidative Functionalization of Late Transition Metal-Carbon Bonds. *Adv. Organomet. Chem.* **2017**, *67*, 221–297.
24. Scheuermann, M.L.; Goldberg, K.I. Reactions of Pd and Pt Complexes with Molecular Oxygen. *Chem. Eur. J.* **2014**, *20*, 14556–14568. [CrossRef] [PubMed]
25. Rudakov, E.S.; Shul'pin, G.B. Stable organoplatinum complexes as intermediates and models in hydrocarbon functionalization. *J. Organomet. Chem.* **2015**, *793*, 4–16. [CrossRef]
26. Watts, D.; Zavalij, P.Y.; Vedernikov, A.N. Consecutive C-H and O_2 Activation at a Pt(II) Center to Produce Pt(IV) Aryls. *Organometallics* **2018**, *37*, 4177–4180. [CrossRef]
27. Miller, B.; Altman, J.; Beck, W. Platinum(IV) complexes of vicinal-1,2-diamines and bis(vicinal-1,2-diamines) with an acylamino function. Evidence for a platinum hydroperoxide intermediate upon oxidation. *Inorg. Chim. Acta* **1997**, *264*, 101–108. [CrossRef]
28. Look, J.L.; Wick, D.D.; Mayer, J.M.; Goldberg, K.I. Autoxidation of Platinum(IV) Hydrocarbyl Hydride Complexes to Form Platinum(IV) Hydrocarbyl Hydroperoxide Complexes. *Inorg. Chem.* **2009**, *48*, 1356–1369. [CrossRef]
29. Khusnutdinova, J.R.; Zavalij, P.Y.; Vedernikov, A.N. Study of aerobic oxidation of phenyl Pt^{II} complexes (dpms)Pt^{II}Ph(L) (dpms = di(2-pyridyl)methanesulfonate; L = water, methanol, or aniline). *Can. J. Chem.* **2009**, *87*, 110–120. [CrossRef]
30. Liu, W.G.; Sberegaeva, A.V.; Nielsen, R.J.; Goddard, W.A.; Vedernikov, A.N. Mechanism of O_2 Activation and Methanol Production by (Di(2-pyridyl)methanesulfonate)$Pt^{II}Me(OH_n)^{(2-n)-}$ Complex from Theory with Validation from Experiment. *J. Am. Chem. Soc.* **2014**, *136*, 2335–2341. [CrossRef]
31. Lippert, B.; Miguel, P.J.S. More of a misunderstanding than a real mismatch? Platinum and its affinity for aqua, hydroxido, and oxido ligands. *Coord. Chem. Rev.* **2016**, *327*, 333–348. [CrossRef]
32. Prokopchuk, E.M.; Jenkins, H.A.; Puddephatt, R.J. Stable cationic dimethyl(hydrido)platinum(IV) complex. *Organometallics* **1999**, *18*, 2861–2866. [CrossRef]
33. Moustafa, M.E.; Boyle, P.D.; Puddephatt, R.J. A biomimetic phenol substituent effect on the reaction of a dimethylplatinum(II) complex with oxygen: Proton coupled electron transfer and multiple proton relay. *Chem. Commun.* **2015**, *51*, 10334–10336. [CrossRef] [PubMed]

34. Fard, M.A.; Behnia, A.; Puddephatt, R.J. Activation of Dioxygen by Dimethylplatinum(II) Complexes. *Organometallics* **2017**, *36*, 4169–4178. [CrossRef]
35. Abo-Amer, A.; Boyle, P.D.; Puddephatt, R.J. Push-pull ligands to enhance the oxygen activation step in catalytic oxidation with platinum complexes. *Inorg. Chim. Acta* **2018**, *473*, 51–59. [CrossRef]
36. Abo-Amer, A.; Boyle, P.D.; Puddephatt, R.J. Push-pull ligands and the oxidation of monomethylplatinum(II) complexes with oxygen or hydrogen peroxide. *Inorg. Chim. Acta* **2020**, *507*, 119580. [CrossRef]
37. Abo-Amer, A.; Boyle, P.D.; Puddephatt, R.J. The remarkable effects of a ligand nitro substituent in organoplatinum chemistry related to activation of dioxygen or reductive elimination of methane. *Polyhedron* **2022**, *217*, 115722. [CrossRef]
38. Behnia, A.; Fard, M.A.; Puddephatt, R.J. Complexes containing a phenol-platinum(II) hydrogen bond: Synthons for supramolecular self-assembly and precursors for hydridoplatinum(IV) complexes. *Eur. J. Inorg. Chem.* **2019**, 2899–2906. [CrossRef]
39. Fard, M.A.; Behnia, A.; Puddephatt, R.J. Platinum(II) complexes of pyridine–amine ligands with phenol substituents: Isotactic supramolecular polymers. *Can. J. Chem.* **2018**, *97*, 238–243. [CrossRef]
40. Fard, M.A.; Behnia, A.; Puddephatt, R.J. Models for cooperative catalysis: Oxidative addition reactions of dimethylplatinum(II) complexes with ligands having both NH and OH functionality. *ACS Omega* **2019**, *4*, 257–268. [CrossRef]
41. Behnia, A.; Fard, M.A.; Puddephatt, R.J. Stereochemistry of oxidative addition of methyl iodide and hydrogen peroxide to organoplatinum(II) complexes having an appended phenol group and the supramolecular chemistry of the platinum(IV) products. *J. Organomet. Chem.* **2019**, *902*, 120962. [CrossRef]
42. Fard, M.A.; Behnia, A.; Puddephatt, R.J. Supramolecular polymer and sheet and a double cubane structure in platinum(IV) iodide chemistry: Solution of a longstanding puzzle. *ACS Omega* **2018**, *3*, 10267–10272. [CrossRef] [PubMed]
43. Fard, M.A.; Puddephatt, R.J. Oxidative addition of halogens to a cycloneophylplatinum(II) complex and evidence for C-H bond activation at platinum(IV). *J. Organomet. Chem.* **2020**, *910*, 121139. [CrossRef]
44. Fard, M.A.; Behnia, A.; Puddephatt, R.J. Cycloneophylplatinum Chemistry: A New Route to Platinum(II) Complexes and the Mechanism and Selectivity of Protonolysis of Platinum-Carbon Bonds. *Organometallics* **2018**, *37*, 3368–3377. [CrossRef]
45. Neugebauer, M.; Schmitz, S.; Brunink, D.; Doltsinis, N.L.; Klein, A. Dynamics of the efficient cyclometalation of the undercoordinated organoplatinum complex $[Pt(COD)(neoPh)]^+$ (neoPh=2-methyl-2-phenylpropyl). *New J. Chem.* **2020**, *44*, 19238–19249. [CrossRef]
46. Campora, J.; Palma, P.; Carmona, E. The chemistry of group 10 metalacycles. *Coord. Chem. Rev.* **1999**, *193*, 207–281. [CrossRef]
47. Griffiths, D.C.; Young, G.B. Mechanisms of thermolytic rearrangement of dineophylplatinum(II) complexes via intramolecular C-H activation. *Organometallics* **1989**, *8*, 875–886. [CrossRef]
48. Ankianiec, B.C.; Hardy, D.T.; Thomson, S.K.; Watkins, W.N.; Young, G.B. Mechanistic studies of the thermolytic and photolytic rearrangement of [bis(diphenylphosphino)ethane]bis(neophyl)platinum(II). *Organometallics* **1992**, *11*, 2591–2598. [CrossRef]
49. SHo, K.Y.; Lam, F.Y.T.; de Aguirre, A.; Maseras, F.; White, A.J.P.; Britovsek, G.J.P. Photolytic Activation of Late-Transition-Metal-Carbon Bonds and Their Reactivity toward Oxygen. *Organometallics* **2021**, *40*, 4077–4091.
50. Griffiths, D.C.; Joy, L.G.; Skapski, A.C.; Wilkes, D.J.; Young, G.B. Rearrangements of neophylplatinum(II) and related derivatives via intramolecular aromatic and aliphatic delta-carbon-hydrogen bond activation—The crystal and molecular-structure of cis-$(Et_3P)_2Pt(CH_2CMe_2Ph)(2\text{-}C_6H_4CMe_3)$. *Organometallics* **1986**, *5*, 1744–1745. [CrossRef]
51. Chappell, S.D.; Cole-Hamilton, D.J. The preparation and properties of metallacyclic compounds of the transition-elements. *Polyhedron* **1982**, *1*, 739–777. [CrossRef]
52. Cámpora, J.; López, J.A.; del Rio, D.; Carmona, E.; Valerga, P.; Graiff, C.; Tiripicchio, A. Synthesis and insertion reactions of the cyclometalated palladium-alkyl complexes $Pd(CH_2CMe_2\text{-}o\text{-}C_6H_4)L_2$.: Observation of a pentacoordinated intermediate in the insertion of SO_2. *Inorg. Chem.* **2001**, *40*, 4116–4126. [CrossRef]
53. Albrecht, M. Cyclometalation Using d-Block Transition Metals: Fundamental Aspects and Recent Trends. *Chem. Rev.* **2010**, *110*, 576–623. [CrossRef]
54. Moustafa, M.E.; Boyle, P.D.; Puddephatt, R.J. Reactivity and mechanism in reactions of methylene halides with cycloneophylplatinum(II) complexes: Oxidative addition and methylene insertion. *J. Organomet. Chem.* **2021**, *941*, 121803. [CrossRef]
55. Ramirez-Jimenez, A.; Gomez, E.; Hernandez, S. Penta- and heptacoordinated tin(IV) compounds derived from pyridine Schiff bases and 2-pyridine carboxylate: Synthesis and structural characterization. *J. Organomet. Chem.* **2009**, *694*, 2965–2975. [CrossRef]
56. Chans, G.M.; Nieto-Camacho, A.; Ramirez-Apan, T.; Hernandez-Ortega, S.; Alvarez-Toledano, C.; Gomez, E. Synthetic, spectroscopic, crystallographic, and biological studies of seven-coordinated diorganotin(IV) complexes derived from Schiff bases and pyridinic carboxylic acids. *Aust. J. Chem.* **2016**, *69*, 279–290. [CrossRef]
57. Iasco, O.; Riviere, E.; Guillot, R.; Buron-LeCointe, M.; Meunier, J.F.; Bousseksou, A.; Boillot, M.-L. $Fe^{II}(pap\text{-}5NO_2)_2$ and $Fe^{II}(qsal\text{-}5NO_2)_2$ Schiff-base spin-crossover complexes: A rare example with photomagnetism and room-temperature bistability. *Inorg. Chem.* **2015**, *54*, 1791–1799. [CrossRef]
58. Sadimenko, A.P. Organometallic complexes of pyridyl Schiff bases. *Adv. Heterocycl. Chem.* **2012**, *107*, 133–218.
59. Liles, D.C.; McPartlin, M.; Tasker, P.A.; Lip, H.C.; Lindoy, L.F. Novel polynuclear cadmium complexes resulting from ring-opening reactions of 2,6-bis(2-R-2-benzoxazolinyl)pyridine (R = Me or H): X-ray structures of $[Cd_4C_{21}H_{17}N_3O_2)_2\cdot(MeCO_2)_4]\cdot Me_2NCHO\cdot H_2O$ and $[Cd_3(C_{19}H_{13}N_3C_2)_2\cdot(MeCO_2)_2\cdot(Me_2NCHO)_2]$. *Chem. Commun.* **1976**, 549–551. [CrossRef]
60. Gurriero, P.; Bullita, E.; Vigato, P.A.; Pelli, B.; Traldi, P. Synthesis, characterization and electron impact mass spectrometry of Schiff bases rearranging to oxazoline, thiazoline and thiazole derivatives. *J. Heterocycl. Chem.* **1988**, *25*, 145–154. [CrossRef]

61. Luo, Y.; Utecht, M.; Dokic, J.; Korchak, S.; Vieth, H.-M.; Haag, R.; Saalfrank, P. Cis-trans isomerisation of substituted aromatic imines: A comparative experimental and theoretical study. *ChemPhysChem* **2011**, *12*, 2311–2321. [CrossRef]
62. Rostovtsev, V.V.; Henling, L.M.; Labinger, J.A.; Bercaw, J.E. Structural and mechanistic investigations of the oxidation of dimethylplatinum(II) complexes by dioxygen. *Inorg. Chem.* **2002**, *41*, 3608–3619. [CrossRef] [PubMed]
63. Ruan, J.; Wang, D.; Kramer, M.J.; Zavalij, P.Y.; Vedernikov, A.N. Oxidation of Methylplatinum(II) Complexes K[(L)Pt^{II}Me] with O_2 and C(sp^3)-X (X = O and C) Reductive Elimination Reactivity of Methylplatinum(IV) Products (*L*)Pt^{IV}Me(OH): The Effect of Structure of Sulfonated CNN-Pincer Ligands L. *Organometallics* **2022**, *41*, 2764–2783.
64. Vedernikov, A.N. Direct Functionalization of M-C (M = Pt-II, Pd-II) Bonds Using Environmentally Benign Oxidants, O_2 and H_2O_2. *Acc. Chem. Res.* **2012**, *45*, 803–813. [CrossRef]
65. Hill, G.S.; Irwin, M.J.; Levy, C.J.; Rendina, L.M.; Puddephatt, R.J.; Andersen, R.A.; McLean, L. Platinum(II) complexes of dimethylsulfide. *Inorg. Synth.* **1998**, *32*, 149–153.
66. Bruker-AXS. *SAINT*, version 2013.8; Bruker-AXS: Madison, WI, USA, 2013.
67. Bruker-AXS. *SADABS*, version 2012.1; Bruker-AXS: Madison, WI, USA, 2012.
68. Sheldrick, G.M. *SHELXT*—Integrated space-group and crystal-structure determination. *Acta Crystallogr. Sect. A Found. Adv.* **2015**, *A71*, 3–8. [CrossRef] [PubMed]
69. GSheldrick, M. Crystal structure refinement with SHELXL. *Acta Crystallogr. Sect. C Struct. Chem.* **2015**, *C71*, 3–8. [CrossRef]
70. Henkelman, G.; Uberuaga, B.P.; Jonsson, H. A climbing image nudged elastic band method for finding saddle points and minimum energy paths. *J. Chem. Phys.* **2000**, *113*, 9901–9904. [CrossRef]
71. Henkelman, G.; Jonsson, H. Improved tangent estimate in the nudged elastic band method for finding minimum energy paths and saddle points. *J. Chem. Phys.* **2000**, *113*, 9978–9985. [CrossRef]
72. Becke, A.D. Density-functional exchange-energy approximation with correct asymptotic behavior. *Phys. Rev. A* **1988**, *38*, 3098–3100. [CrossRef]
73. Andzelm, J.; Kolmel, C.; Klamt, A. Incorporation of solvent effects into density-functional calculations of molecular energies and geometries. *J. Chem. Phys.* **1995**, *103*, 9312–9320. [CrossRef]
74. ADF 2020, SCM, Vrije Universiteit, Amsterdam, The Netherlands. Available online: https://www.scm.com (accessed on 1 January 2021).